Atmospheric Environment 215 (2019) 116813

Contents lists available at ScienceDirect

Atmospheric Environment

journal homepage: www.elsevier.com/locate/atmosenv

Light scattering from volcanic-sand particles in deposited and aerosol form

Nataliya Zubko[a,*], Olga Muñoz[b], Evgenij Zubko[c], Maria Gritsevich[d,e], Jesús Escobar-Cerezo[d], Matthew J. Berg[f], Jouni Peltoniemi[a]

[a] Finnish Geospatial Research Institute, Geodeetinrinne 2, 02430, Masala, Finland
[b] Instituto de Astrofísica de Andalucía, CSIC Glorieta de la Astronomía s/n, 18008, Granada, Spain
[c] Kyung Hee University, Humanitas College, Yongin-shi, Kyungki-do 17104, Republic of Korea
[d] University of Helsinki, Department of Physics, Gustaf Hällströmin katu 2, 00014, Helsinki, Finland
[e] Institute of Physics and Technology, Ural Federal University, Mira street 19, 620002, Ekaterinburg, Russia
[f] Kansas State University, Department of Physics, 1228 North 17th Street, Manhattan, KS, 66506-2601, USA

ARTICLE INFO

Keywords:
Volcanic sand
Remote sensing
Polarimetry
Radiometry
Photometry
Particulate surface
Aerosols
Light scattering
Discrete dipole approximation
Refractive index
Soot

ABSTRACT

The light-scattering properties of volcanic sand collected in Iceland are studied here to characterize the sand particles and develop a reference for future remote-sensing observations. While such sand is common in Iceland, the smaller-size fraction can be readily transported by winds and found in the atmosphere at distant locations. The sand appears dark when deposited on a surface due to the high optical absorption of the material. Therefore, atmospheric regions containing such particles during a dust storm may absorb sunlight considerably, causing redistribution of solar energy. Here, we measure the angular scattered-light intensity and degree of linear polarization from the sand. This is done with two experimental apparatuses, the Cosmic Dust Laboratory (CoDuLab) at the Institute de Astrofísica de Andalucía (IAA) and the goniospectropolarimeter (FIGIFIGO) at the Finnish Geospatial Research Institute (FGI). Two scattering-scenarios of practical interest for remote-sensing applications are considered: (1) single sand-particles suspended in aerosol as an optically thin cloud, and (2) the same particles deposited on a substrate. We also model the measurements with the discrete dipole approximation to estimate the complex-valued refractive index m, where we find that $m \approx 1.6 + 0.01i$ at $\lambda = 647$ nm. Lastly, we present a comparative analysis of the polarimetric response of the sand particles with that reported in the literature for carbon-soot, another highly absorbing atmospheric contaminant.

1. Introduction

One of the largest uncertainties with regard to the interaction of solar radiation between the atmosphere and the Earth-surface, i.e., the Earth's radiative energy budget, is associated with aerosols including dust (Boucher et al., 2013). This work studies Icelandic volcanic sand, a significant source of dust in Northern Europe that is close to arctic glacier (Prospero et al., 2012). In particular, our study reveals a degree of similarity between the optical properties of Icelandic volcanic sand and black carbon particles; specifically, both particle types strongly absorb solar radiation thus heating the atmosphere and reducing the amount of solar energy received at the Earth surface. The majority of black carbon in the atmosphere has anthropogenic origin, while the volcanic sand discussed here is natural in origin. Given its history of volcanic activity, Iceland has experienced an extended period of absorbing-aerosol effects as evidenced by the abundance of volcanic sand, which has led to climatic influences both locally and regionally across the northern latitudes.

Volcanic sand is one of the main dust-sources in Iceland due to the abundance of rock of volcanic origin. The weather conditions are favorable for active sand-formation via the erosion of solidified lava flows, and thus, about 20% of Iceland is covered with volcanic sand (Arnalds, 2015). Sandy deserts cover large portions of the south coast and glacial margins of the active volcanic zone from the Mýrdalsjökull glacier to areas northeast of the Vatnajökull glacier (Fig. 1). The desert area near the Mýrdalsjökull glacier can be seen in the enlarged MODIS satellite image along with a visible portion of the contaminated glacier. For a more detailed map of the sand dessert distribution, see Arnalds, 2015 (chapter 11).

Volcanic sand in Iceland consist mostly of basaltic glass (Arnalds, 2015). Such basaltic volcanic materials can be found in other volcanically active areas such as Hawaii and other states of the USA and in New Zealand (Edgett and Lancaster, 1993), however the composition, particle size distribution, and microphysical properties vary with the

* Corresponding author.
E-mail address: nataliya.zubko@nls.fi (N. Zubko).

https://doi.org/10.1016/j.atmosenv.2019.06.051
Received 30 January 2019; Received in revised form 31 May 2019; Accepted 24 June 2019
Available online 03 July 2019
1352-2310/

Fig. 1. Satellite image of Iceland obtained with MODIS (Blue Marble from August 2004). Enlarged image of the selected area is taken from MODIS 08.07.2009). (For interpretation of the references to color in this figure legend, the reader is referred to the Web version of this article.)

place of origin and sand formation factors. It is also worth noting that Iceland has one of the largest volcaniclastic sand-fields (Arnalds et al., 2001).

Frequent dust-storms lift small volcanic-sand particles off the surface and transport them over great distances. For instance, they can be deposited in high latitude regions like Svalbard and Greenland (Groot Zwaaftink et al., 2017). Unlike desert sand, which is typically a quartz-mineral (e.g., Volten et al., 2001; Nousiainen, 2009), the composition of volcanic sand is less well known. Nevertheless, what is known about the composition of suspended volcanic sand suggests a significant impact on the atmosphere, specifically across the Northern latitudes (Dagsson-Waldhauserova et al., 2016) in addition to its contribution to accelerating glacier melt (Wittmann et al., 2017).

The transport of volcanic sand by wind contaminates both the atmosphere and ground-surface along its transport path, where suspended particles efficiently absorb solar radiation leading to simultaneous heating of the atmosphere and surface. Because the suspended particles eventually settle-out, for instance, on a pure ice and/or snow surface, the surface albedo is altered leading to enhanced heating and an increase in the surface's density (Meinander et al., 2014; Peltoniemi *et al.*, 2015). This in turn triggers melting or evaporation of ice and snow surfaces (Qian et al., 2009).

Contamination of the atmosphere or icy/snow terrestrial surfaces by volcanic sand can be detected with remote-sensing techniques through ground-based and satellite observations (e.g. AERONET, Holben et al., 1998, Sinyuk et al., 2007, GOME-2: Munro et al. 2016, CALIOP/CALIPSO: Winker et al., 2009). The reflectance and polarization of sunlight scattered by atmospheric aerosols contain important information about the microphysical properties of the particles. Indeed, polarimetry is a powerful and promising tool for the retrieval and characterization of these microphysical properties. Presently, several space instruments have polarization sensors and provide Earth observational data (e.g. Herman, 2005; Munro et al. 2016). Moreover, a number of new space missions are planned, which will perform airborne polarimetry (Dubovik et al., 2019). Interpretation of such measurements, however, remains difficult primarily because the measurements are simultaneously affected by the particles' shape, size distribution, and chemical composition. Comparison of satellite data with ground-based measurements may show significant differences. An example is Tao et al. (2017), who demonstrate an evaluation of the MODIS Deep Blue aerosol algorithm in the desert region of East Asia and compare to retrievals with ground-based observations obtained with China Aerosol Remote Sensing Network. They find that the MODIS-based retrievals of aerosol optical depth can be significantly underestimated. Besides the aerosol optical depth characteristics, aerosol-type classification is another challenge (Kahn and Gaitley, 2015). For instance, a set of dust mixtures is used to define the aerosol type in Multiangle Imaging Spectroradiometer (MISR) retrievals algorithms. Thus, knowledge of the optical properties of various dust types is critical for the success of such retrievals. Laboratory studies of the light scattering properties of dust particles could meaningfully improve the algorithm inputs and interpretation of *in situ* measurements.

In this work, we investigate the reflectance and degree of linear polarization of sunlight scattered by volcanic-sand particles suspended in air and the same particles deposited on a surface. As such, our experiment reproduces both of measurement scenarios relevant for remote-sensing observations of volcanic sand, i.e., in the atmosphere or deposited on an ice/snow surface. Previous related measurements mainly focus on either single-particles or deposited-particles (Muñoz et al., 2004, Dabrowska et al., 2015; Hadamcik, 2002; Sun et al., 2014; Peltoniemi et al., 2009, Wilkman et al., 2016). There are only few examples where both light-scattering scenarios are simultaneously studied (e.g., Shkuratov et al., 2004, Shkuratov et al., 2006; Mirvatte et al., 2011) and Icelandic volcanic sand is not encompassed in that work. The measurements in our work are conducted at two experimental facilities: the goniospectropolariphotometer (FIGIFIGO) located at the Finnish Geospatial Research Institute (FGI) and Cosmic Dust Laboratory (CoDuLab) at the Instituto de Astrofísica de Andalucía (IAA). The FIGIFIGO facility (Fig. 2) is designed to measure the light-scattering response from a particle-coated surface (Peltoniemi et al., 2014), whereas the CoDuLab facility (Fig. 3) is used to measure the full scattering-matrix of particles suspended in air (Muñoz et al., 2012). We also complement our study with mass spectrometry to infer the elemental composition of the volcanic sand samples used.

Light scattering properties of surface-deposited volcanic sand have, in part, been studied before. In Peltoniemi et al. (2015a,b), the sand is used as a highly absorbing contaminant for a snow surface, where that study focus on how the contamination affects the reflection and polarization properties of the snow. In work by Zubko et al. (2016), the optical properties of high-contrast two-component mixtures involving volcanic sand are studied, where the sand serves as a dark component among two types of bright components, salt (NaCl) and ferric sulfate ($Fe_2(SO_4)_3$). Note, however, that the light-scattering behavior of volcanic sand is investigated in these studies only when the particles are deposited on a substrate (particulate surface). The single-particle regime of light scattering is not yet investigated.

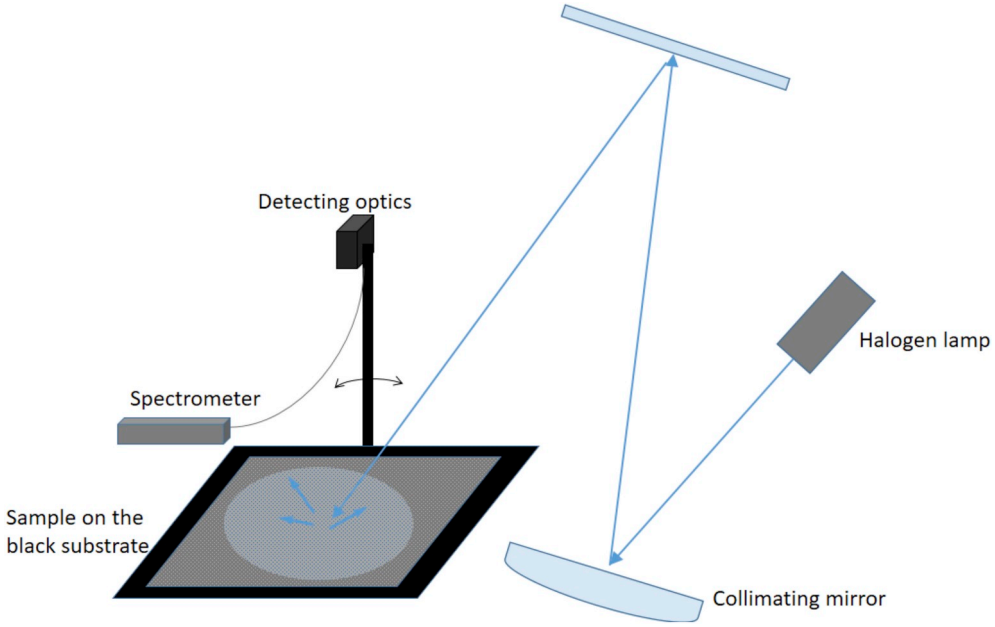

Fig. 2. Scheme of Finnish Geospatial Research Institute goniospectropolariphotometer FIGIFIGO setup.

2. Sample description

Volcanic-sand particles mainly consist of poorly crystallized glasses of basaltic to andesitic origin. The samples we consider are a mixture of glaciofluvial volcanic ash originating from beneath the Mýrdalsjökull glacier mixed with ash from the Eyjafjallajökull and Grímsvötn eruptions of 2010 and 2011, respectively. We choose this sample because it is representative of materials that are typical of aerosol-dust sources in Southern Iceland and the particles deposited on glaciers or snow in that area (Arnalds et al., 2013, Arnalds et al., 2016). Specifically, our samples were collected from the Mýrdalssandur area in Iceland. The large black-colored area in Fig. 1 corresponds to the field of volcanic sand and the upper layer of this sand (about 10 cm thickness) was collected with a shovel. Wind erosion in the area contributes to the redistribution of loose surface material, and according to Arnalds, 2015), the rates of surface transport of aeolian materials is between 500 and 3,000 kg m^{-1} $year^{-1}$. This means that about 0.5–3 tons are blown over a 1 m wide transect each year. The relevant volcanic sand formation and erosion processes in Iceland are outlined in more detail, in e.g., (Baratoux et al. 2011; Arnalds et al. 2013).

Our sand samples generally divide into the following categories:

1) Natural volcanic sand without processing (except for drying);
2) Sieved volcanic sand where the size of the particles is less than 250 μm, including:
   a) Dry sand;
   b) Wet sand, where moisture is provided by an atomizer;
3) Milled volcanic sand where the particles are ground to produce a fine-grained powder.

Samples 1–2 are studied with the FIGIFIGO experimental apparatus only. The natural sample (1) is abundant with coarse, millimeter-sized particles. Unfortunately, with the CoDuLab apparatus, such particles are too large for a feasible study of their light-scattering behavior at the single-particle level. The problem arises primarily from the aerosol generator, which becomes jammed by such large particles. The sieved volcanic sand (2) consists of particle sizes < 170 μm is used in the CoDuLab experiments, although the signal-to-noise ratios (SNRs) are low. The poor SNRs can be explained as follows: First, many of the sub-millimeter sieved samples remain too large for optimal operation of the

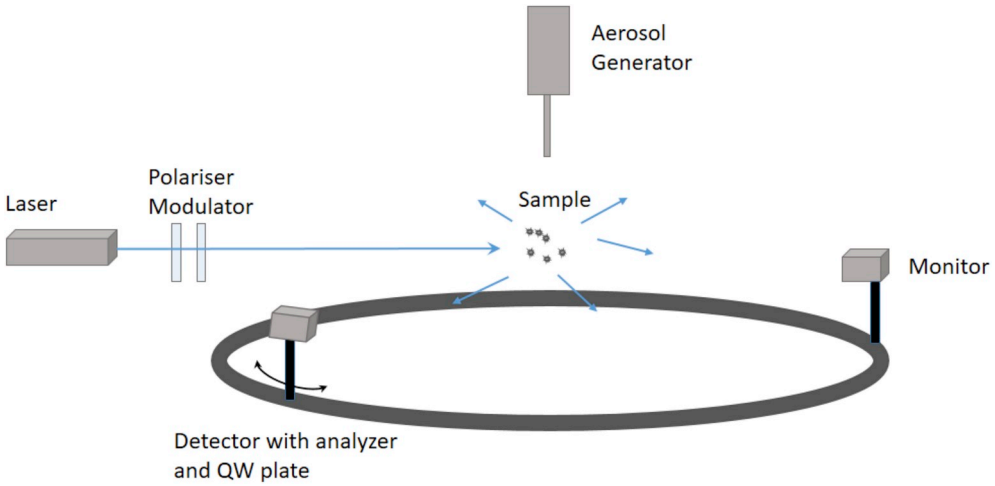

Fig. 3. Scheme of IAA Cosmic Dust Laboratory setup.

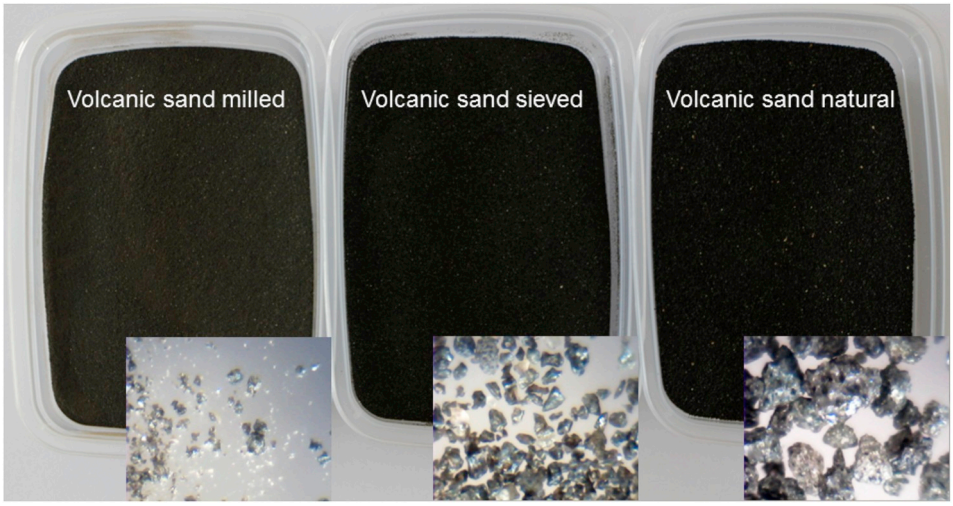

Fig. 4. Appearance of milled, sieved, and natural volcanic sand samples along with optical-microscope images of the same samples.

aerosol generator. Although the generator operates considerably better with sample (2) than sample (1), the amount of suspended dust remains low leading to weak scattering-signals. Second, due to the large size of the constituent particles, they are much darker in appearance compared to the smaller, micron-sized particles and this can be seen in Fig. 4. Indeed, the milled sample (3) exhibits a brighter appearance in Fig. 4 compared to samples (1) and (2). Optical-microscope images of the samples are included in Fig. 4 to highlight the variability of particle sizes and shapes.

To obtain a more detailed view of the particle morphology in the natural sand sample (1), the particles are also examined by scanning electron microscopy (SEM) at various magnifications, see Fig. 5. As seen, the particles exhibit a highly irregular and somewhat vesicular morphology. The elemental composition of these particles is analyzed with X-ray spectrometry and the results are presented in Fig. 6. The analysis is repeated for particles of different sizes and it is notable that no significant variation in the chemical composition is found.

The size distribution of the milled volcanic sand sample (3) is shown in Fig. 7. The distribution is measured at the IAA CoDuLab with the *MasterSizer2000* instrument by *Malvern Scientific*. Note that the *MasterSizer2000* measures the flux of laser light scattered at a several scattering angles θ near forward-scattering direction. To retrieve information about the particles, it is customary to fit such measurements with the two methods: Fraunhofer-diffraction theory or Mie theory (Bohren and Huffman, 1983). As neither of these theories applies well to highly irregular particle shapes in general, the fitting procedure can yield results with error, e.g., with respect to particle size.

What emerges from Fig. 7 is that for particle radii > 0.25–0.3 μm, both approaches reveal a power-law size distribution r^{-n} that can be fit by $n = 3.5$ in the Fraunhofer framework and at $n = 3.2$ in the Mie

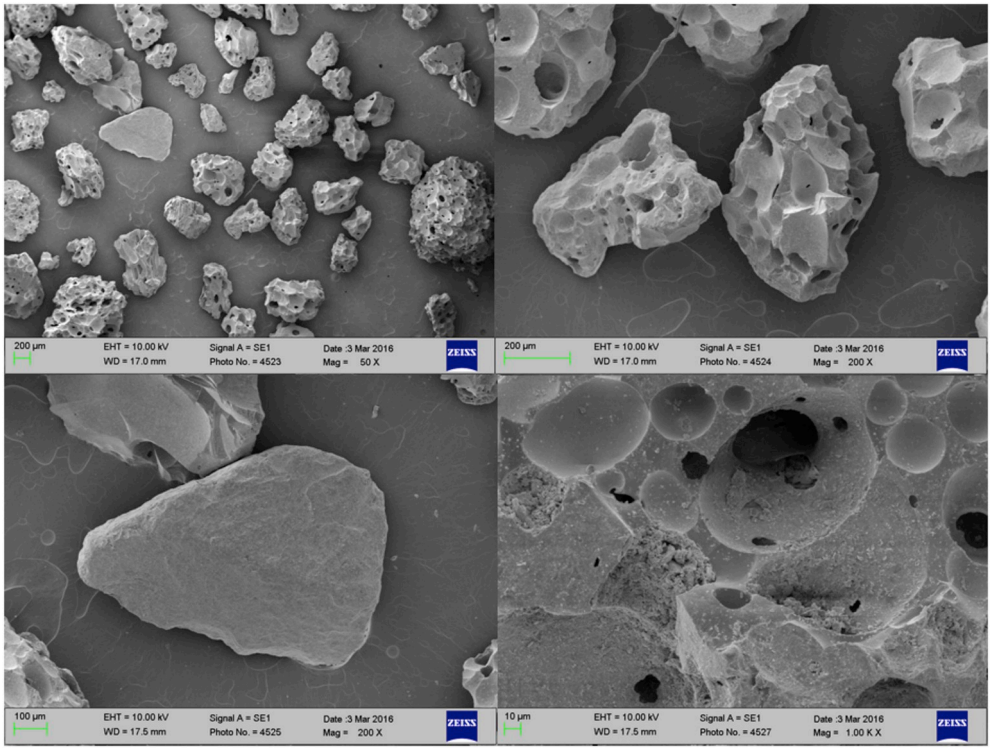

Fig. 5. Scanning electron microscopic images of the natural sample.

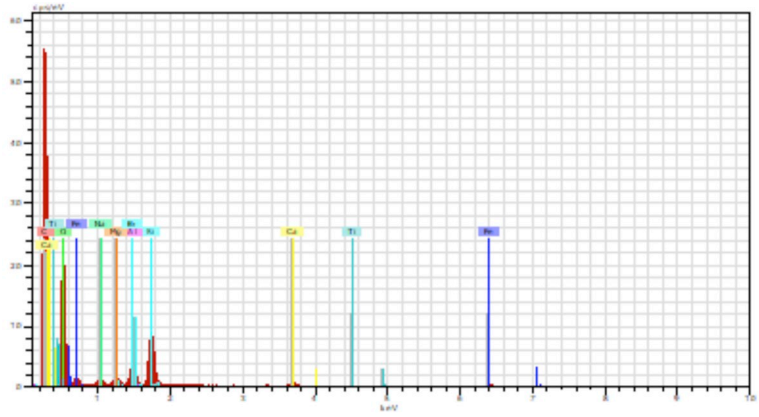

Spectrum: volcanic sand 80

Element	Series	unn. C [wt.%]	norm. C [wt.%]	Atom. C [at.%]	Error (1 Sigma) [wt.%]
Oxygen	K-series	47.80	27.32	25.33	5.23
Iron	K-series	10.74	6.14	1.63	0.51
Silicon	K-series	9.61	5.49	2.90	0.42
Aluminium	K-series	1.23	0.70	0.39	0.08
Calcium	K-series	2.93	1.68	0.62	0.13
Titanium	K-series	1.52	0.87	0.27	0.08
Magnesium	K-series	0.88	0.50	0.31	0.07
Sodium	K-series	0.81	0.46	0.30	0.07
Bromine	L-series	3.21	1.84	0.34	0.17
Carbon	K-series	96.23	55.00	67.92	10.19
Total:		174.97	100.00	100.00	

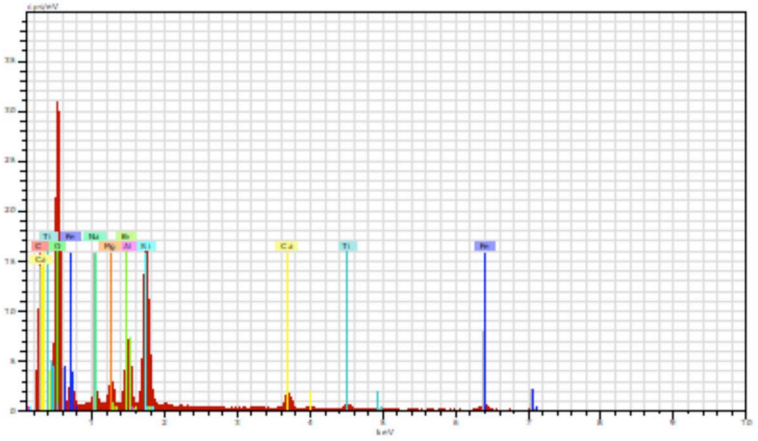

Spectrum: volcanic sand 81

Element	Series	unn. C [wt.%]	norm. C [wt.%]	Atom. C [at.%]	Error (1 Sigma) [wt.%]
Carbon	K-series	25.94	19.11	30.99	3.11
Oxygen	K-series	53.60	39.49	48.07	5.94
Iron	K-series	19.06	14.04	4.90	0.88
Silicon	K-series	17.68	13.02	9.03	0.75
Aluminium	K-series	2.40	1.77	1.28	0.14
Calcium	K-series	5.01	3.69	1.79	0.20
Titanium	K-series	3.13	2.30	0.94	0.14
Magnesium	K-series	1.79	1.32	1.06	0.12
Sodium	K-series	1.50	1.11	0.94	0.12
Bromine	L-series	5.62	4.14	1.01	0.28
Total:		135.72	100.00	100.00	

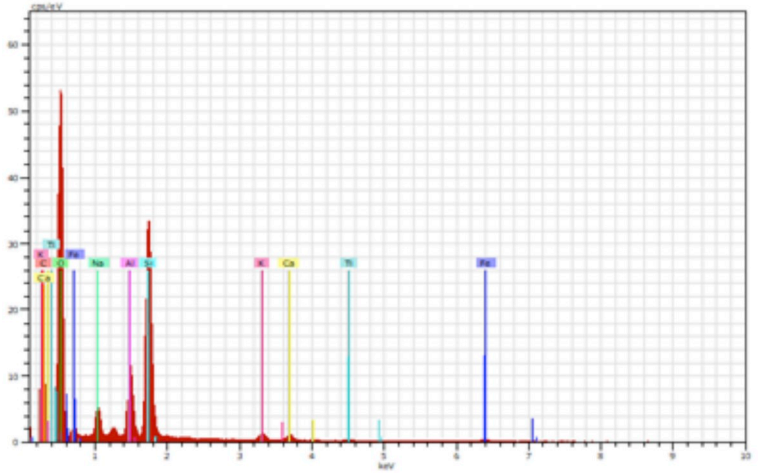

Spectrum: volcanic sand 82

Element	Series	unn. C [wt.%]	norm. C [wt.%]	Atom. C [at.%]	Error (1 Sigma) [wt.%]
Carbon	K-series	32.63	24.14	34.68	3.70
Oxygen	K-series	59.74	44.20	47.67	6.44
Iron	K-series	6.94	5.14	1.59	0.35
Silicon	K-series	23.91	17.69	10.87	1.00
Aluminium	K-series	5.39	3.99	2.55	0.27
Calcium	K-series	1.82	1.35	0.58	0.09
Sodium	K-series	2.52	1.87	1.40	0.18
Potassium	K-series	1.29	0.96	0.42	0.07
Titanium	K-series	0.90	0.67	0.24	0.06
Total:		135.15	100.00	100.00	

Figure 6. Element composition of natural volcanic sand particles analyzed with the X-ray spectrometry.

approach. However, we stress that both approaches assume idealistic targets (spherical particles) and therefore, the results should be taken with caution when applied to the highly irregular particles here. This point will cause some uncertainty in the retrievals of the size distribution that should be taken into account.

3. Experimental facilities and measurement details

3.1. FIGIFIGO

The Finnish Geodetic Institute goniospectropolariphotometer FIGIFIGO (Fig. 2) is designed to measure the reflectance and degree of linear polarization of various surfaces, both in the laboratory and in the field conditions (e.g. Peltoniemi et al., 2015b). A detailed description of the FIGIFIGO can be found in Peltoniemi et al. (2014). In our study, the sample is deposited on the surface by uniform sprinkling particles on a black substrate with a layer of 0.8–1 cm thick. The measurements are taken in the principal plane, i.e., when the surface normal lies within the scattering plane and to improve the SNR we repeat the measurements 25 times. To compare phase-angle dependences of the reflectance and the degree of linear polarization of FIGIFIGO with CoDuLab measurements, we present FIGIFIGO results obtained in the waveband λ = 642–652 nm (hereafter λ = 647 nm). The maximum uncertainty, ~3%, appears in the polarimetric measurements at some phase angles whereas the average uncertainty in the polarimetric response is ~2%. The uncertainty in the measurements of reflectance is noticeably lower compared to that of the polarimetric measurements.

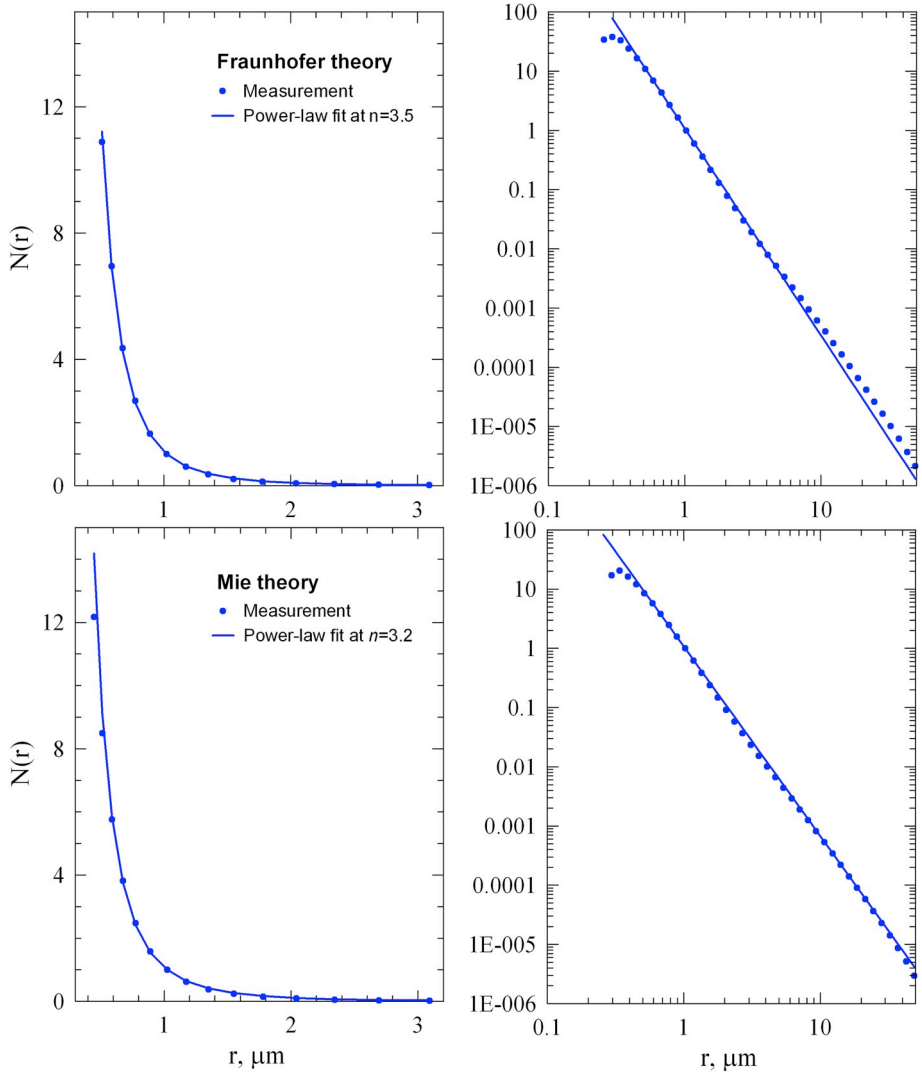

Fig. 7. Size distribution of the milled volcanic sand particles on linear scale on the right and log scale on the left.

3.2. CODULAB

The IAA Cosmic Dust Laboratory (CoDuLab) is designed to measure the light scattering response from aerosol particles, see Fig. 3. We notice that in the case of irregularly shaped particles, the light-scattering response can be described by the so-called (4 × 4) *scattering matrix* or the *Mueller matrix* consisting of six non-zero elements (see, e.g., Bohren and Huffman, 1983):

$$F = \begin{pmatrix} F_{11} & F_{12} & 0 & 0 \\ F_{12} & F_{22} & 0 & 0 \\ 0 & 0 & F_{33} & F_{34} \\ 0 & 0 & -F_{34} & F_{44} \end{pmatrix} \quad (1)$$

Using the CoDuLab facility, one can measure all six non-zero elements over the *scattering angle* θ range from 3° to 177° at several wavelengths. In our study, we investigate the upper block of non-zero elements. For a detailed description of the CoDuLab facility refer to (Muñoz et al., 2012).

The results presented here are obtained at $\lambda = 647$ nm. In particular, we measure the F_{11} and F_{12} elements of the scattering matrix for the milled volcanic sand sample (3). The intensity of the scattered sunlight I and its degree of linear polarization P are defined via the elements of the scattering matrix as follows: $I \propto F_{11}$, $P = -F_{12}/F_{11}$.

4. Results and discussion

4.1. Reflectance and degree of linear polarization

We first investigate the difference in light scattering behavior for the sieved sample deposited on a surface in dry and wet conditions by measuring the reflectance and degree of linear polarization as a function of λ. Spectra for the wet and dry samples at $\theta = 170°$ and $\theta = 140°$ are shown in Fig. 8. The reflectance of the wet sample is found, on average, to be nearly half of that for the dry sample. Moreover, the shape of the reflectance curve clearly depends on presence of water, which is especially noticeable for λ in the range 500–1000 nm. The reflectance plot demonstrates the highly absorbing property of volcanic sand evidenced by the maximum value being only ~0.044 at $\lambda = 650$ nm. The strongest reflectance response is observed for the dry sample at $\theta = 170°$. Note, that while the reflectance spectra of this sample differs unambiguously at the two scattering angles ($\theta = 170°$ and $\theta = 140°$), a similar difference for the wet sample is less in magnitude.

In contrast to the reflectance spectra, the curve shapes and scattering response of the polarization spectra are not as sensitive to water content. As shown later, however, a discrimination between wet and dry particles is easier at smaller θ. On the other hand, the degree of linear polarization decreases as the scattering angle grows. This is

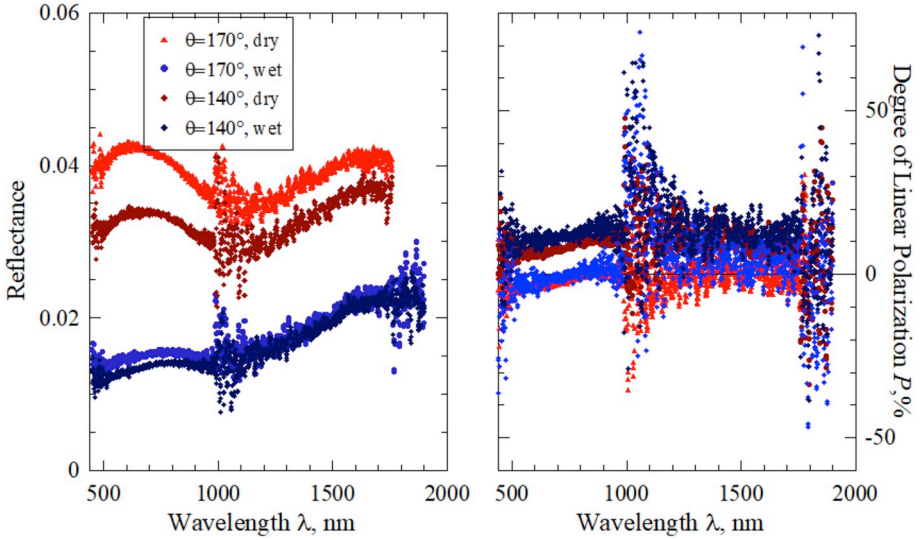

Fig. 8. Reflectance and degree of linear polarization as function of wavelength of sieved wet and dry volcanic sand particles deposited on the surface.

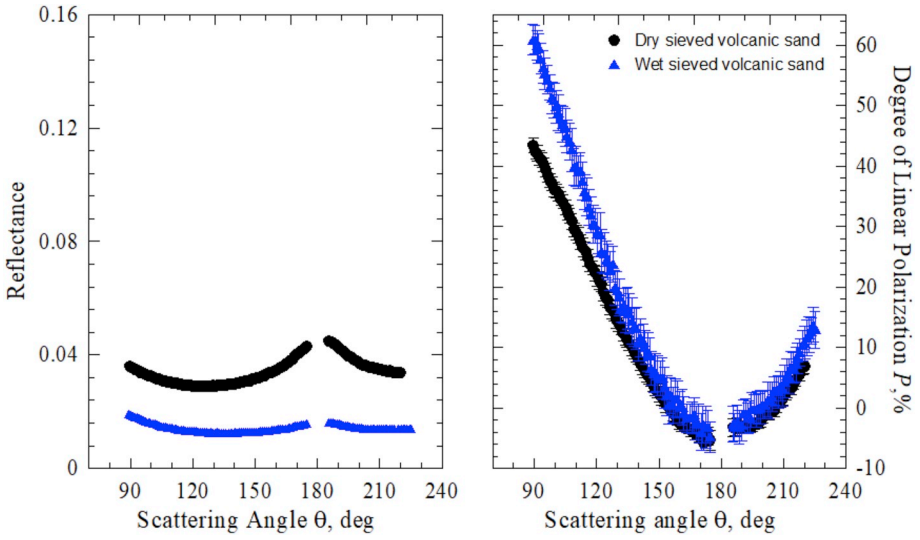

Fig. 9. Reflectance and degree of linear polarization of the dry and wet sieved volcanic sand as a function of scattering angle at wavelength of 647 nm.

better seen in the angular dependence of the polarization in the wet and dry samples shown in Fig. 9, where the measurements are taken at $\lambda = 647$ nm. We see that the reflectance of the wet sample (blue curve) decreases considerably whereas the polarimetric response becomes noisier. In the latter case, however, the polarimetric response for the wet sample (blue curve) is higher compared to the dry sample (black curve). The difference between the dry and wet samples is best seen at side scattering, $\theta \sim 90^{\circ}$. Also, the increase of uncertainty in our measurements can be explained by the continuous evaporation of water during the measurements. To minimize the effect due to evaporation, we replenish the water content in the sample several times during the course of the experiment with water atomizer.

Particle size is a dominate factor affecting the light-scattering behavior of a sample, which is illustrated in Fig. 10 for reflectance and polarization at $\lambda = 647$ nm. Here, the natural and milled volcanic sand samples (1) and (3), respectively, are illuminated at $\theta = 148^{\circ}$. Near the backscattering direction, i.e., $\theta \rightarrow 180^{\circ}$, the reflectance of the milled sample appears to be considerably higher than that of the natural sample. This change is consistent with the so-called *Umov effect* or *Umov law*, which is the inverse correlation between reflectance near backscattering, i.e., geometric albedo, and the maximum value that the degree of linear polarization may acquire, e.g., see Shkuratov and Opanasenko (1992); Zubko et al. (2016). According to the Umov effect, greater polarization is expected from the natural sand compared to the milled sand. Indeed, the maximum degree of linear polarization of the milled sample is ~2.5 times less than that for the natural sample. Also note, that the value of negative polarization near the backscattering direction is greater for the milled sample. The Umov effect can be seen for the near-backscattering reflectance and polarization maximum for the dry and wet sieved samples presented in Fig. 9.

Comparing the reflectance of the dry sieved samples shown in Fig. 9 with the reflectance for the natural and milled samples in Fig. 10, one finds that the reflectance of the sieved sample is greater than the natural sand and less than the milled sand. Correspondingly, the polarization of the sieved sample is smaller than for the natural sand and greater than the milled sand.

Comparative analysis of the light-scattering behavior for deposited particles and the same type of particles suspended in air as an "optically thin cloud," i.e., as an aerosol, can provide important information needed for the interpretation of observations of atmosphere and underlying terrain. The milled volcanic sand is measured in both scenarios, i.e., deposited on a surface or as an aerosol, and the results are shown in Fig. 11. Note that for the aerosol, it is not feasible to measure an absolute flux of the scattered light. Therefore, we normalize the

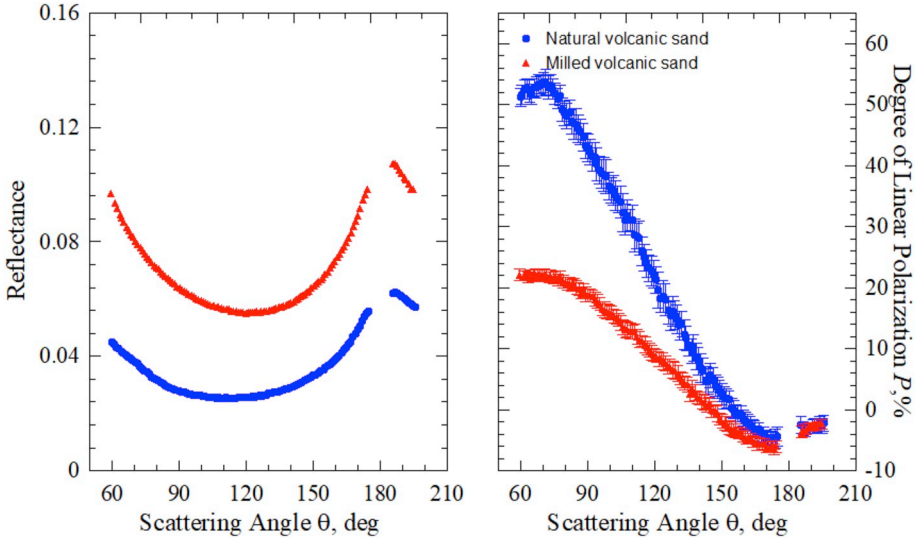

Fig. 10. Reflectance and degree of linear polarization of the dry natural and milled volcanic sand as function on phase angle at wavelength of 647 nm.

reflectance data at $\theta = 90^{\circ}$. In the FIGIFIGO measurements, the deposited particles are illuminated at $\theta = 52^{\circ}$ with respect to the surface normal. Due to measurement constraints on the θ range and the increased intensity of scattered light from single particles near the forward-scattering direction, our analysis is limited to the range $60^{\circ} < \theta < 177^{\circ}$.

In Fig. 11, one can see that the normalized reflectance for the aerosol is noticeably stronger for small θ compared to the data for deposited particles. However, the aerosol data also show a decrease and become weaker for $\theta > 90^{\circ}$. The maximum value of the degree of linear polarization appears greater for deposited particles compared to the aerosol, i.e., $P_{max} \approx (22.07 \pm 0.93)\%$ at $\theta_{max} \approx 60^{\circ}$ and $P_{max} \approx (18.7 \pm 1.1)\%$ at $\theta_{max} \approx 100^{\circ}$, respectively. Although this difference is not large, it is detected with confidence in Fig. 11. For $\theta < 105^{\circ}$, this finding qualitatively differs from that reported in Shkuratov et al. (2007), for example, where ten different samples are investigated including clay, olivine, feldspar, and volcanic ash. All those samples reveal a systematically lower polarization for deposited samples. Our results, however, are in a good agreement with soot measurements by Mirvatte et al., 2011, where polarization measured from surface packed particles considerably exceeds that from the aerosol particles. Notice in Fig. 11 that the negative polarization branch near backscattering for deposited particles appears deeper than the aerosol, which is opposite to the conclusions drawn in Shkuratov et al. (2004). This difference could result from specific features of our sample of volcanic sand. It is significant, for example, that our sand is much darker in appearance than any sample used in Shkuratov et al. (2004, 2007).

The light scattering response for volcanic sand differs considerably from other types of sand such as desert sand, which is obvious from their visual appearance. While volcanic sand is dark in appearance (its geometric albedo is ~0.05), desert sands are considerably brighter.

In Fig. 12 we plot the normalized reflectance (left) and degree of linear polarization (right) as a function of scattering angle for three different samples: white-clay, milled volcanic-sand, and the ash particles from the Eyjafjallajokull volcano. The light scattering properties of white clay and volcanic ash were studied with CODULAB by Munoz et al. in 2011 and Merikallio et al. in 2015. Here we present a comparison of the light scattering properties of volcanic sand in this study to the white clay and Eyjafjallajokull volcanic ash samples. White clay

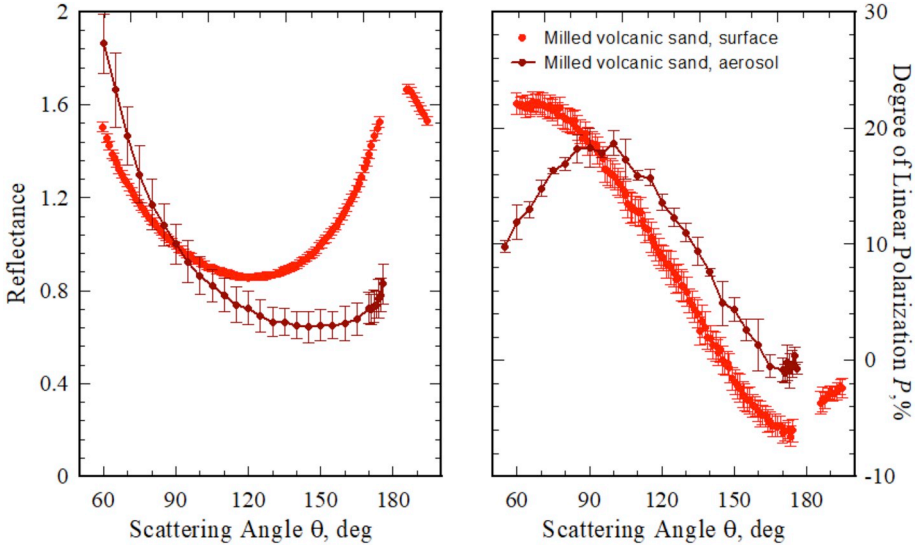

Fig. 11. The scattering angle dependence of the normalized reflectance and degree of linear polarization obtained for the surface and aerosol of the milled volcanic sand.

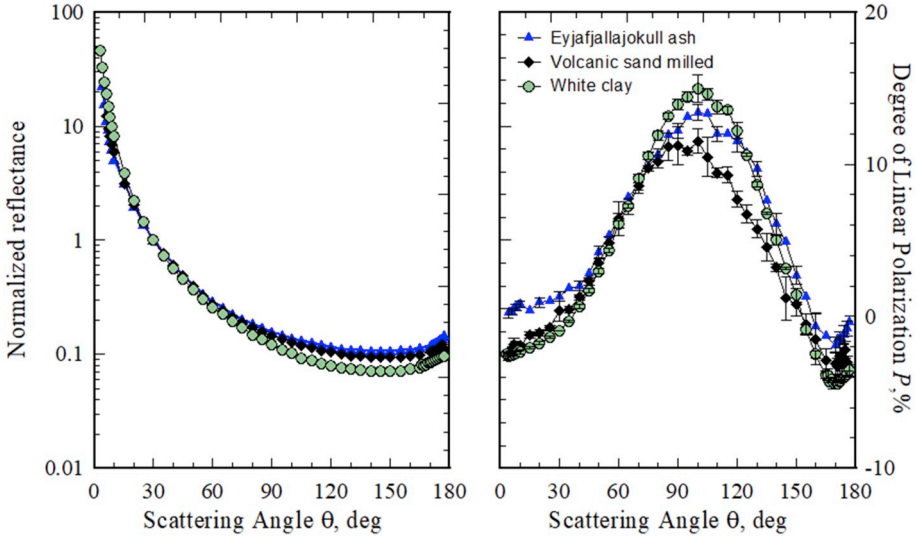

Fig. 12. The normalized reflectance and degree of linear polarization as a function of scattering angle for three different samples: white-clay, milled volcanic-sand, and the ash particles from the Eyjafjallajokull volcano.

mainly consists of illite, kaolinite, montmorillonite, quartz and is an important component of aerosols in the atmosphere. Eyjafjallajokull volcanic ash was collected at 5 km from the source after the April 2010 eruption, where the main constituent is silica, SiO_2. These particle also contain Al_2O_3, CaO, TiO_2, FeO, MgO and Na_2O.

As one can see from Fig. 12 there is similarity between the three polarization curves. The refractive index m of the Eyjafjallajokull ash particles could be similar to that in the milled volcanic sand. However, they should differ significantly from that of the white clay, at least with regard to the imaginary part, Im(m). Nevertheless, the light scattering response of white-clay particles resembles that of the volcanic sand and ash particles. The resemblance could be explained by a difference in size distribution of the white-clay and volcanic sand and ash particles that, by coincidence, compensates the difference in refractive index. The angular profiles of the reflectance at large scattering-angles ($> 90^{\circ}$) clearly differs for the dark samples (volcanic sand and ash) and light samples, i.e., the white clay. Such a feature could be useful in passive remote-sensing of aerosol particles.

Fig. 13 compares our results to the polarization measurements

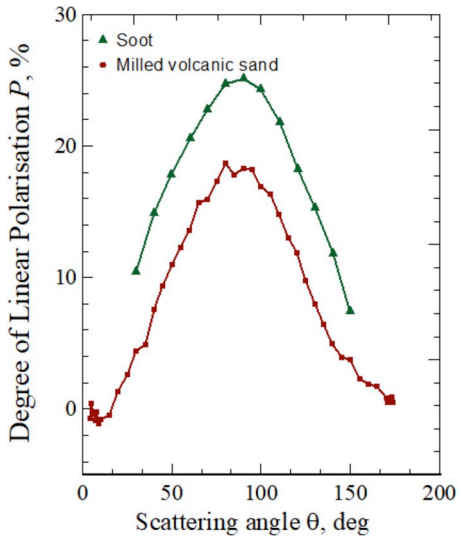

Fig. 13. Comparison of the polarization response of volcanic sand $\lambda = 647$ nm and soot particles at $\lambda = 632.8$ nm (data adopted from Mirvatte et al., 2011) suspended into the air.

obtained for levitated soot-particles by Mirvatte et al., 2011. The data adopted from Mirvatte et al., 2011 is measured at $\lambda = 632.8$ nm from a dense cloud of levitated agglomerated particles of Polymethyl Methacrylate (PMMA), hereafter called the soot sample. The soot particles are micrometer-sized aggregates, where the constituent grains have a diameter of several tens of nm. The maximum polarization of the volcanic sand is about 19%, while the soot is about 25%. Based on this, and considering the Umov law, we can conclude that the near-back-scattering reflectance of the soot sample is lower than that of milled volcanic sand.

4.2. Constraint of the complex refractive index of volcanic sand

An advantage of our study with single-scattering particles is that interpretation data does not involve common complications due multiple scattering. We can develop a quantitative model describing the single-scattering particles based on a numerically exact solution of the Maxwell equations, although this cannot be done here for the deposited particles. The ultimate goal of such modeling is retrieval of the microphysical properties of the particles.

In general, light scattering by submicron and micron-sized particles is dependent on their size distribution, shape, and complex refractive index (m). However, Zubko *et al.* (2015) show that in the case of highly irregular particles, the effect of size distribution and m on the light scattering behavior dominates the effects of particle shape. Furthermore, the size distribution of the milled volcanic sand is constrained by the *MasterSizer2000* measurements (Fig. 7) and this allows us to estimate m for the volcanic sand with the light-scattering model.

Specifically, we model the angular profiles of the scattered intensity I and degree of linear polarization P for the milled volcanic-sand particles using the so-called *agglomerated debris particles* method (Zubko, 2015; Zubko et al. 2015). Such particles have a disordered morphology with a packing density of the constituent material being ~0.236. Six examples of the agglomerated debris particles are shown in Fig. 14, which are generated by systematically damaging a perfect sphere as described in Zubko et al. (2013). An notable feature of the model particles is that they reproduce analogous laboratory measurements of a variety of samples similar to those considered here, such as feldspar (Zubko et al., 2013), forsterite (Zubko, 2015), and olivine (Videen et al., 2018). In particular, the model parameters, i.e., the size distribution and m, applied to these analogous measurements closely match the actual microphysical characteristics of the samples.

Analysis of satellite data is typically done with spheroidal model-

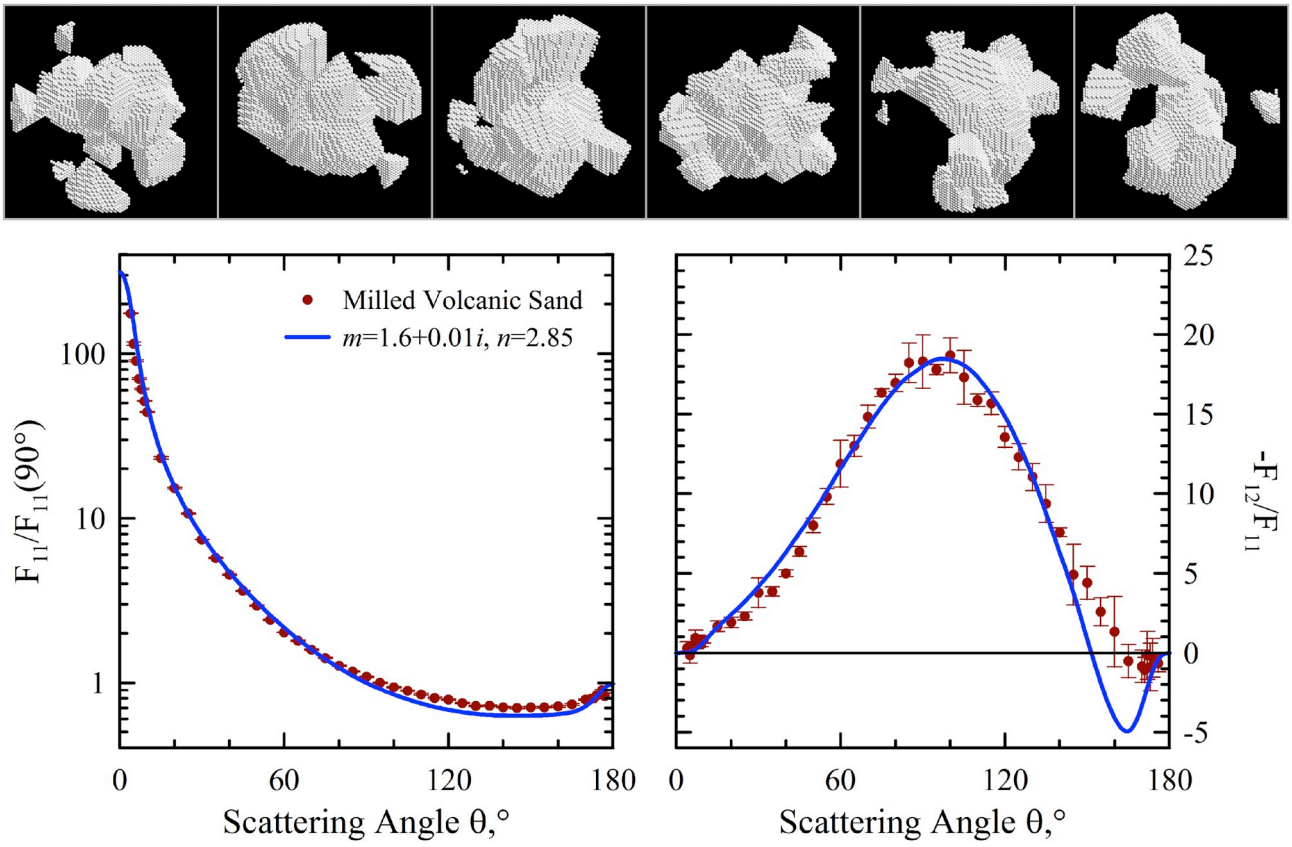

Fig. 14. On the top: Six examples of the modeled agglomerated debris particles. On the bottom: Intensity I (left) and degree of linear polarization P (right) as a function of the scattering angle θ in the milled volcanic sand and their model (blue curve) at $n = 2.85$ and $m = 1.6 + 0.01i$. (For interpretation of the references to color in this figure legend, the reader is referred to the Web version of this article.)

particles, see for example Dubovik et al. However, Dubovik et al., (2006) shows that the use of spheroidal particles could not satisfactorily reproduce laboratory measurements when multiple wavelengths are involved. Furthermore, the microphysical properties retrieved with spheroidal particles do not match the true properties of the feldspar particles (refractive index, size, and aspect-ratio distributions), while agglomerated debris particles is in good quantitative agreement with the true microphysical characteristics of feldspar (Zubko et al., 2013).

A particle's light-scattering behavior depends, in part, on the ratio of its radius r to wavelength λ, is commonly called the size parameter $x = 2\pi r/\lambda$ (Bohren and Huffman, 1983). In application to an irregularly shaped particle, we assign r to a sphere that circumscribes the model particle used. Then, we compute the relevant light-scattering quantities using agglomerated debris particles for $1 < x < 32$ with the *discrete dipole approximation* (DDA). The DDA is a flexible technique designed for numerical simulation of light scattering by particles with an arbitrary shape (Yurkin and Hoekstra, 2007). In the DDA framework, the particle is replaced by a set of cubic cells that reproduces the shape and internal structure, where the size of the cells d is sufficiently small compared to λ. As demonstrated in Zubko et al. (2010), the DDA yields robust numerical results for $2\pi d|m|/\lambda \leq 1$. Each cell is then approximated by an electric dipole and, thus, the integral equation describing interaction of an electromagnetic wave with the particle is transformed into a system of linear algebraic equations. This system of equations is then solved via an iterative method. In order to comply with the discretization criterion for d above, we consider two cases for each agglomerated debris particle: $64 \times 64 \times 64$ cells and $128 \times 128 \times 128$ cells. The former is used when $x \leq 15$ and the latter when $x > 15$. The size parameter is varied in steps of $\Delta x = 1$ for $1 < x < 15$ and $\Delta x = 2$ for $16 < x < 32$. Given that $\lambda = 647$ nm in our study, this size-parameter range corresponds to a particle-size range $0.1\,\mu m < r < 3.3\,\mu m$. As demonstrated in Zubko et al. (2013), Zubko (2015), and Videen et al. (2018), such a range is sufficient to reproduce the light-scattering response in a polydisperse system exhibiting a power-law size distribution with an exponent of $n \geq 2.9$.

To investigate the dependence on m, we apply the DDA to agglomerated debris particles at 46 values of m, with real and imaginary parts spanning the ranges $1.1 < \mathrm{Re}(m) < 2.43$ and $0 < \mathrm{Im}(m) < 1$, respectively. For every pair (x, m) we average the light-scattering response over a minimum of 500 random shapes to ensure a statistically reliable result. We also perform size averaging using a power-law distribution r^{-n} over the full range of r considered. Initial values for n are inferred from Fig. 7, i.e., $n = 3.2$ and 3.5. However, we do not consider these as precisely known values. Instead, we assume a degree of variation of ± 0.5, which recognizes the uncertainty inherent to the size distribution measurements with the *MasterSizer 2000* instrument.

We investigate all the available refractive indices, searching for the best fit to the maximum value of the degree of linear polarization $P_{max} \approx (18.7 \pm 1.1)\%$ found for the milled-sand sample at $\theta = 100^{\circ}$. When such fit is possible, we then compare the entire angular profiles of I and P measured for the given sample with that from the DDA model applied to agglomerated debris particles (Zubko et al., 2013; Zubko, 2015; Videen et al., 2018). As Fig. 14 shows, the best fit for $\lambda = 647$ nm is obtained for $m = 1.6 + 0.01i$ and $n = 2.85$. As one can see, the intensity is reproduced well for all θ, whereas the degree of linear polarization tends to agree less near backscattering ($\theta > 140^{\circ}$) where the phenomenon of negative polarization is observed (i.e., $I_{\perp} < I_{||}$). The same qualitative behavior is seen for a feldspar particle (Zubko et al., 2013), although the difference is smaller. Overall, the agglomerated debris particle model in other work closely matches the true microphysical properties of the measured particle (Zubko et al., 2013; Zubko, 2015; Videen et al., 2018). Such performance of the model lends

confidence to our conclusion in Fig. 14 that $m = 1.6 + 0.01i$ for the volcanic sand at $\lambda = 647$ nm.

Finally, consider the question of how the inferred material absorption, i.e., Im(m) = 0.01, corresponds to the dark appearance of the milled volcanic sand, having a reflectance ~ 0.1 near backscattering $\theta = 175^\circ$ and presumably ~ 0.12 at $\theta = 180^\circ$ (see Fig. 11). We draw attention to previous laboratory measurements of m in powdered kerogen type-II reported by Khare et al. (1990). In particular, for the red part of the spectrum, a similar value for Im(m) is found, Im(m) ≈ 0.012, whereas the powder is described as having the dark appearance. Thus, our finding that Im (m) = 0.01 for the volcanic sand agrees well with the visual appearance of the sand deposited on a surface.

5. Conclusions

Our study of the light-scattering behavior of Icelandic volcanic sand achieves a quantitative characterization of this important material. The reflectance and polarization deposited sand strongly depends on the particle size-distribution. According to the Umov law, the maximum of the polarization degree encodes information on the material's optical absorption and reflectance. This effect is demonstrated for the three samples of volcanic sand containing particles with different size distributions. The degree of linear polarization differs by nearly a factor of three between the milled and natural-sand samples whereas the polarization seen for the sieved sample is smaller than the natural sand and greater than the milled sand. However, the water added to the sieved sand increases its polarimetric response considerably, so that at some scattering angles the response is nearly the same as the natural sand, which consists of larger particles. This observation may have important implications for remote-sensing observations of regions with such sand present.

Our comparative analysis of the reflectance and polarization response of particles suspended as an aerosol with those deposited on a surface reveal:

(1) The normalized reflectance of light scattered by the aerosols is noticeably stronger at small scattering-angles compared to that of the deposited particles.
(2) The positive degree of linear polarization for the aerosols is greater than for the deposited particles for $90^\circ < \theta < 160^\circ$.
(3) The maximum polarization is as large as $P_{max} \approx 22\%$ occurring at $\theta_{max} \approx 60^\circ$ for deposited particles, and $P_{max} \approx 19\%$ at $\theta_{max} \approx 100^\circ$ for the aerosol particles.
(4) The polarization response from the aerosol and deposited particles becomes similar at $\theta = 95^\circ$.
(5) The negative polarization branch of deposited particles is deeper than that of the aerosol.

Finally, based on discrete-dipole modeling of the reflectance and degree of linear polarization we estimate the refractive index of the Icelandic volcanic sand to be $m = 1.6 + 0.01i$ at $\lambda = 647$ nm.

Acknowledgments

This research was partially supported by the Academy of Finland Project no. 260027 and the COST Action MP1104 “Polarization as a tool to study the Solar System and beyond”. NZ acknowledges Magnus Ehrnrooth Foundation for the research travel support. This work also has been partially supported by contracts AYA2015-67152-R and RTI2018-095330-B-I00. We thank P. Dagsson Waldhauserová, O. Arnalds, A. Virkkula, O. Meinander, and J. Svensson for their help obtaining the samples and for relevant discussions. We acknowledge the use of imagery provided by services from NASA's Global Imagery Browse Services (GIBS), part of NASA's Earth Observing System Data and Information System (EOSDIS). We also would like to thank reviewers for their constructive reviews.

References

Arnalds, O., Dagsson-Waldhauserova, P., Olafsson, H., Aeolian Research, 2016. The Icelandic volcanic aeolian environment: Processes and impacts — A review. 176-195 20, 176–195. https://doi.org/10.1016/j.aeolia.2016.01.004.
Arnalds, O., Gisladottir, F.O., Sigurjonsson, H., 2001. Sandy deserts of Iceland: an overview. J. Arid Environ. 47, 359–371. https://doi.org/10.1006/jare.2000.0680.
Arnalds, O., Thorarinsdottir, E.F., Thorsson, J., Waldhauserova, P.D., Agustsdottir, A.M., 2013. An extreme wind erosion event of the fresh Eyjafjallajökull 2010 volcanic ash. Sci. Rep. 3. https://doi.org/10.1038/srep01257.
Arnalds, O., 2015. The Soils of Iceland, World Soils Book Series. Springer Netherlands. https://doi.org/10.1007/978-94-017-9621-7.
Baratoux, D., Mangold, N., Arnalds, O., Bardintzeff, J.-M., Platevoët, B., Grégoire, M., Pinet, P., 2011. Volcanic sands of Iceland – diverse origins of aeolian sand deposits revealed at Dyngjusandur and Lambahraun. Earth Surf. Process. Landforms 36, 1789–1808. https://doi.org/10.1002/esp.2201.
Bohren, C.F., Huffman, D.R., 1983. Absorption and Scattering of Light by Small Particles. Wiley, New York.
Boucher, O., Randall, D., Artaxo, P., Bretherton, C., Feingold, G., Forster, P., Kerminen, V.-M., Kondo, Y., Liao, H., Lohmann, U., Rasch, P., Satheesh, S.K., Sherwood, S., Stevens, B., Zhang, X.Y., 2013. Clouds and aerosols. In: Stocker, T.F., Qin, D., Plattner, G.-K., Tignor, M., Allen, S.K., Boschung, J., Nauels, A., Xia, Y., Bex, V., Midgley, P.M. (Eds.), Climate Change 2013: the Physical Science Basis. Contribution of Working Group I to the Fifth Assessment Report of the Intergovernmental Panel on Climate Change. Cambridge University Press, Cambridge, United Kingdom and New York, NY, USA.
Dabrowska, D., Muñoz, O., Moreno, F., Ramos, J.L., Martínez-Frías, J., Wurm, G., 2015. Scattering matrices of martian dust analogs at 488 nm and 647 nm. Icarus 250, 83–94. https://doi.org/10.1016/j.icarus.2014.11.024.
Dagsson-Waldhauserova, P., Magnusdottir, A., Olafsson, H., Arnalds, O., 2016. The spatial variation of dust particulate matter concentrations during two Icelandic dust storms in 2015. Atmosphere 7, 77. https://doi.org/10.3390/atmos7060077.
Dubovik, O., Li, Z., Mishchenko, M.I., et al., 2019. J. Quant. Spectrosc. Radiat. Transfer 224, 474–511.
Dubovik, O., Sinyuk, A., Lapyonok, T., Holben, B.N., Mishchenko, M., Yang, P., Eck, T.F., Volten, H., Muñoz, O., Veihelmann, B., van der Zande, W.J., Leon, J.-F., Sorokin, M., Slutsker, I., 2006. Application of spheroid models to account for aerosol particle nonsphericity in remote sensing of desert dust. J. Geophys. Res. 111, D11208. https://doi.org/10.1029/2005JD006619.
Edgett, K.S., Lancaster, N., 1993. Volcaniclastic aeolian dunes: terrestrial examples and application to martian sands. J. Arid Environ. 25, 271–297.
Groot Zwaaftink, C.D., Arnalds, Ó., Dagsson-Waldhauserova, P., Eckhardt, S., Prospero, J.M., Stohl, A., 2017. Temporal and spatial variability of Icelandic dust emissions and atmospheric transport. Atmos. Chem. Phys. 17, 10865–10878. https://doi.org/10.5194/acp-17-10865-2017.
Hadamcik, E., 2002. Polarization of light scattered by fluffy particles (PROGRA2 experiment). Icarus 155, 497–508. https://doi.org/10.1006/icar.2001.6732.
Herman, M., 2005. Aerosol remote sensing from POLDER/ADEOS over the ocean: improved retrieval using a nonspherical particle model. J. Geophys. Res. 110, D10S02. https://doi.org/10.1029/2004JD004798.
Holben, B.N., Eck, T.F., Slutsker, I., Tanré, D., Buis, J.P., Setzer, A., Vermote, E., Reagan, J.A., Kaufman, Y.J., Nakajima, T., Lavenu, F., Jankowiak, I., Smirnov, A., 1998. AERONET—A Federated Instrument Network and Data Archive for Aerosol Characterization. Remote Sensing of Environment 66 (1), 1–16. https://doi.org/10.1016/S0034-4257(98)00031-5.
Kahn, R.A., Gaitley, B.J., 2015. An analysis of global aerosol type as retrieved by MISR. J. Geophys. Res. Atmos. 120, 4248–4281. https://doi.org/10.1002/2015JD023322.
Khare, B.N., Thompson, W.R., Sagan, C., Arakawa, E.T., Meisse, C., Gilmour, I., 1990. Optical constants of kerogen from 0.15 to 40 mm: comparison with meteoritic organics. In: Proceedings of Lunar and Planetary Science Conference, vol. XXI. pp. 627–628.
Meinander, O., Kontu, A., Virkkula, A., Arola, A., Backman, L., Dagsson-Waldhauserová, P., Järvinen, O., Manninen, T., Svensson, J., de Leeuw, G., Leppäranta, M., 2014. Brief communication: light-absorbing impurities can reduce the density of melting snow. Cryosphere 8, 991–995. https://doi.org/10.5194/tc-8-991-2014.
Merikallio, S., Muñoz, O., Sundström, A.-M., Virtanen, T.H., Horttanainen, M., Leeuw, G., Nousiainen, T., 2015. Optical modeling of volcanic ash particles using ellipsoids. J. Geophys. Res. 120 (9), 4102–4116. https://doi.org/10.1002/2014JD022792.
Muñoz, O., Volten, H., Hoveneir, J.W., veihelmann, B., van der Zande, W.J., Waters, L.B.F.M., Rose, W.I., 2004. Scattering matrices of volcanic ash particles of mount st. Helens, redoubt, and mount spurr volcanoes. J. Geophys. Res. 109 Issue D16, Cite ID D16201.
Muñoz, O., Moreno, F., Guirado, D., Ramos, J.L., Volten, H., Hovenier, J.W., 2011. The IAA cosmic dust laboratory: experimental scattering matrices of clay particles. Icarus 211, 894–900.
Mirvatte, F., Renard, J-B., Hadamcik, E., Couté, B., Gaubicher, B., Jeannot, M., 2011. New studies on scattering properties of different kinds of soot and carbon-black. Journal of Quantitative Spectroscopy and Radiative Transfer 112, 1766–1775. https://doi.org/10.1016/j.jqsrt.2011.01.009.
Muñoz, O., Moreno, F., Guirado, D., Dabrowska, D.D., Volten, H., Hovenier, J.W., 2012. The amsterdam–granada light scattering database. J. Quant. Spectrosc. Radiat. Transf. 113, 565–574. https://doi.org/10.1016/j.jqsrt.2012.01.014.
Munro, R., Lang, R., Klaes, D., Poli, G., Retscher, C., Lindstrot, R., et al., 2016. The GOME-2 instrument on the Metop series of satellites: instrument design, calibration, and level 1 data processing –an overview. Atmos. Meas. Tech. 9, 1279–1301. https://doi.

org/10.5194/amt- 9- 1279- 2016.
Peltoniemi, J., Hakala, T., Suomalainen, J., Puttonen, E., 2009. Polarised bidirectional reflectance factor measurements from soil, stones, and snow. J. Quant. Spectrosc. Radiat. Transf. 110, 1940–1953. https://doi.org/10.1016/j.jqsrt.2009.04.008.
Peltoniemi, J.I., Hakala, T., Suomalainen, J., Honkavaara, E., Markelin, L., Gritsevich, M., Eskelinen, J., Jaanson, P., Ikonen, E., 2014. Technical notes: a detailed study for the provision of measurement uncertainty and traceability for goniospectrometers. J. Quant. Spectrosc. Radiat. Transf. 146, 376–390. https://doi.org/10.1016/j.jqsrt.2014.04.011.
Nousiainen, T., 2009. Optical modeling of mineral dust particles: A review. Journal of Quantitative Spectroscopy and Radiative Transfer 110 (14–16), 1261–1279. https://doi.org/10.1016/j.jqsrt.2009.03.002.
Peltoniemi, J.I., Gritsevich, M., Hakala, T., Dagsson-Waldhauserová, P., Arnalds, Ó., Anttila, K., Hannula, H.-R., Kivekäs, N., Lihavainen, H., Meinander, O., Svensson, J., Virkkula, A., de Leeuw, G., 2015a. Soot on Snow experiment: bidirectional reflectance factor measurements of contaminated snow. Cryosphere 9, 2323–2337. https://doi.org/10.5194/tc-9-2323-2015.
Peltoniemi, J.I., Gritsevich, M., Puttonen, E., 2015b. Reflectance and Polarization Characteristics of Various Vegetation Types//Springer Praxis Books, vol. 9. pp. 257–294. Light Scattering and Radiative Transfer, Light Scattering Reviews. https://doi.org/10.1007/978-3-642-37985-7_7.
Prospero, J.M., Bullard, J.N., Hodgkins, R., 2012. High-latitude dust over the north atlantic: inputs from Icelandic proglacial dust storms. Science 335 (6072), 1078–1082. https://doi.org/10.1126/science.1217447.
Qian, Y., Gustafson Jr., W.I., Leung, L.R., Ghan, S.J., 2009. Effects of soot-induced snow albedo change on snowpack and hydrological cycle in western United States based on Weather Research and Forecasting chemistry and regional climate simulations. J. Geophys. Res. 114. https://doi.org/10.1029/2008jd011039.
Shkuratov, Y., Bondarenko, S., Ovcharenko, A., Pieters, C., Hiroi, T., Volten, H., Munoz, O., Videen, G., 2006. Comparative studies of the reflectance and degree of linear polarization of particulate surfaces and independently scattering particles. Journal of Quantitative Spectroscopy & Radiative Transfer 100, 340–358. https://doi.org/10.1016/j.jqsrt.2005.11.050.
Shkuratov, YuG., Opanasenko, N.V., 1992. Polarimetric and photometric properties of the moon: telescope observation and laboratory simulation. II – the positive polarization. Icarus 99, 468–484. https://doi.org/10.1016/0019-1035(92)90161-Y.
Shkuratov, Y., Ovcharenko, A., Zubko, E., Volten, H., Muñoz, O., Videen, G., 2004. The negative polarization of light scattered from particulate surfaces and of independently scattering particles. J. Quant. Spectrosc. Radiat. Transf. 88, 267–284. https://doi.org/10.1016/j.jqsrt.2004.03.029.
Shkuratov, Yu, Bondarenko, S., Kaydash, V., Videen, G., Muñoz, O., Volten, H., 2007. Photometry and polarimetry of particulate surfaces and aerosol particles over a wide range of phase angles. J. Quant. Spectrosc. Radiat. Transfer 106, 487–508. https://doi.org/10.1016/j.jqsrt.2007.01.031.
Sinyuk, A., Dubovik, O., Holben, B., Eck, T.F., Bréon, F.-M., Martonchik, J., et al., 2007. Simultaneous retrieval of aerosol and surface properties from a combination of AERONET and satellite data. Remote Sens. Environ. 107, 90–108. https://doi.org/10.1016/j.rse.2006.07.022.
Sun, Z., Zhang, J., Tong, Z., Zhao, Y., 2014. Particle size effects on the reflectance and negative polarization of light backscattered from natural surface particulate medium: soil and sand. J. Quant. Spectrosc. Radiat. Transf. 133, 1–12. https://doi.org/10.1016/j.jqsrt.2013.03.013.
Tao, M., Chen, L., Wang, Z., Wang, J., Che, H., Xu, X., et al., 2017. Evaluation of MODIS Deep Blue aerosol algorithm in desert region of East Asia: ground validation and intercomparison. J. Geophys. Res.: Atmosphere 122. https://doi.org/10.1002/2017JD026976 10, 357–10, 368.
Videen, G., Zubko, E., Arnold, J.A., MacCall, B., Weinberger, A.J., Shkuratov, Yu, Muñoz, O., 2018. On the interpolation of light-scattering responses from irregularly shaped particles. J. Quant. Spectrosc. Radiat. Transfer 211, 123–128. https://doi.org/10.1016/j.jqsrt.2018.03.009.
Volten, I., Munoz, O., de Haan, J.F., Vassen, W., Hovenier, J.W., Muinonen, K., Nousiainen, T., 2001. Scattering matrices of mineral aerosol particles at 441.6 and 632.8 nm. Journal of Geophysical Research : Atmospheres 106 (D15), 17375–17401. https://doi.org/10.1029/2001JD900068.
Wilkman, O., Gritsevich, M., Zubko, N., Peltoniemi, J., Muinonen, K., 2016. Photometric modelling for laboratory measurements of dark volcanic sand//. J. Quant. Spectrosc. Radiat. Transf. 185, 37–47. https://doi.org/10.1016/j.jqsrt.2016.08.013.
Winker, D.M., Vaughan, M.A., Omar, A., Hu, Y., Powell, K.A., Liu, Z., et al., 2009. Overview of the CALIPSO mission and CALIOP data processing algorithms. J. Atmos. Ocean. Technol. 26, 2310–2323. https://doi.org/10.1175/2009JTECHA1281.1.
Wittmann, M., Groot Zwaaftink, C.D., Steffensen Schmidt, L., Guðmundsson, S., Pálsson, F., Arnalds, O., Björnsson, H., Thorsteinsson, T., Stohl, A., 2017. Impact of dust deposition on the albedo of Vatnajökull ice cap, Iceland. Cryosphere 11, 741–754. https://doi.org/10.5194/tc-11-741-2017.
Yurkin, M.A., Hoekstra, A.G., 2007. The discrete dipole approximation: An overview and recent developments. Journal of Quantitative Spectroscopy and Radiative Transfer 106 (1–3), 558–589. https://doi.org/10.1016/j.jqsrt.2007.01.034.
Zubko, E., 2015. Modeling light scattering by forsterite particles. Opt. Lett. 40, 1204–1207. https://doi.org/10.1364/OL.40.001204.
Zubko, E., Petrov, D., Grynko, Ye, Shkuratov, Yu, Okamoto, H., Muinonen, K., Nousiainen, T., Kimura, H., Yamamoto, T., Videen, G., 2010. Validity criteria of the discrete dipole approximation. Appl. Opt. 49, 1267–1279. https://doi.org/10.1364/AO.49.001267.
Zubko, E., Muinonen, K., Muñoz, O., Nousiainen, T., Shkuratov, Yu, Sun, W., Videen, G., 2013. Light scattering by feldspar particles: comparison of model agglomerate debris particles with laboratory samples. J. Quant. Spectrosc. Radiat. Transfer 131, 175–187. https://doi.org/10.1016/j.jqsrt.2013.01.017.
Zubko, E., Shkuratov, Yu, Videen, G., 2015. Effect of morphology on light scattering by agglomerates. J. Quant. Spectrosc. Radiat. Transfer 150, 42–54. https://doi.org/10.1016/j.jqsrt.2014.06.023.
Zubko, N., Gritsevich, M., Zubko, E., Hakala, T., Peltoniemi, J.I., 2016. Optical measurements of chemically heterogeneous particulate surfaces. J. Quant. Spectrosc. Radiat. Transf. 178, 422–431. https://doi.org/10.1016/j.jqsrt.2015.12.010.